ACS APPLIED MATERIALS & INTERFACES

Research Article

www.acsami.org

Interconnected Network of $CoMoO_4$ Submicrometer Particles As High Capacity Anode Material for Lithium Ion Batteries

Christie T. Cherian, M. V. Reddy, Sow Chorng Haur, and B. V. R. Chowdari*

Department of Physics, National University of Singapore, Singapore, 117551

ABSTRACT: Interconnected networks of $CoMoO_4$ submicrometer particles are prepared by thermolysis of polymer matrix based metal precursor solution. The material exhibited a high reversible capacity of 990 (±10) mAh g^{-1} at a current density of 100 mA g^{-1}, with 100% capacity retention between 5 and 50 cycles. The improved electrochemical performance of $CoMoO_4$ submicrometer particles with interconnected network like morphology makes it promising as a high-capacity anode material for rechargeable lithium ion batteries.

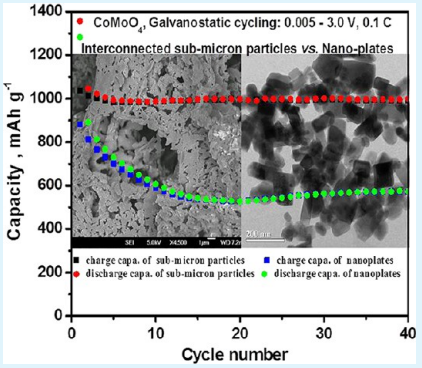

KEYWORDS: *cobalt molybdate, polymer matrix based precursor method, citric acid assisted microwave method, anode, Li-ion battery*

Lithium ion batteries (LIBs) are the most rapidly growing high-energy storage device used in portable electronic devices such as mobile phones, digital cameras, and laptops, etc.[1] LIBs have also been considered as a prospective battery system in hybrid electric vehicles due to their high volumetric and gravimetric capacity, enabling smaller and lighter battery packs.[2] Large specific capacity can be achieved by utilizing all possible oxidation states of a compound through the "conversion reaction" or displacement redox reaction in which the transition metal oxides/fluorides/nitrides can reversibly react with lithium to form corresponding metal nanoparticles embedded in Li_2O/LiF/Li_3N matrix.[3,4] Molybdenum-containing mixed oxides can be considered as prospective anode materials due to the ability of the metal ions to exist in several oxidation states in these oxides, ranging from 3^+ to 6^+ for Mo and reversibly reacting with Li delivering high capacity, at potentials lower than 2 V.[5−8] Molybdenum can form stable oxides with many metals with stoichiometry, $MeMoO_4$, where Me = Co, Zn, Mn, Cu, Ni, Mg, Pb, Ca, Fe, Cd.[9−13]

MoO_3 is a well-known lithium insertion material and can accommodate a maximum of 1.5 lithium per molybdenum atom with theoretical capacity of ∼280 mAh g^{-1}, in the voltage range 1.5−3.5 V.[14,15] In the potential window of 0.0−3.0 V vs Li, MoO_3 has been found to participate in conversion reaction, reversibly cycling 4−6 mols of Li, delivering high capacity in the range 745−1115 mAh g^{-1}.[5,16] Hence MoO_3 can be considered as potential cathode as well as anode material for LIBs. Li-cycling properties of various metal molybdates have also been explored by several research groups. Leyzerovich et al. studied the Li intercalation of lithium in various ternary metal molybdates such as $CuMoO_4$, $ZnMoO_4$, $NiMoO_4$, and $FeMoO_4$ in the voltage range 0.5−3.0 V and all those compounds were found to be unsatisfactory as electrode materials for lithium ion rechargeable batteries due to rapid capacity fading.[17] Kim et al. investigated the electrochemical performance of $MnMoO_4$ in the voltage range 0.0−2.0 V and observed a discharge capacity of 1800 mAh g^{-1} accompanied by large irreversible capacity and amorphization during first cycle.[18] Nidhi et al. examined the anodic performance of $CaMoO_4$ and found that 5% carbon coated $CaMoO_4$ deliver a stable capacity of 400 mAh g^{-1} up to 40 cycles, when cycled in the voltage range 0.005−2.5 V at a current of 60 mA g^{-1}.[15]

Among various metal molybdates, $CoMoO_4$ has received much research interest due to its photocatalytic, magnetic, and electrochemical properties.[19,20] To the best of our knowledge, there is no report of achieving stable capacity for α-$CoMoO_4$ when tested as anode material for LIBs. Three compounds of different structure with the same stoichiometry, $CoMoO_4$, are known to form under atmospheric pressure: the low temperature α-phase (α-$CoMoO_4$), the high temperature β-isomorph (β-$CoMoO_4$), and the hydrate ($CoMoO_4{\cdot}nH_2O$).[21,22] Co^{2+} is in octahedral sites in all these isomorphs whereas Mo^{6+} is in octahedral coordination in α-$CoMoO_4$ and in tetrahedral coordination in β phase and hydrate phase. Since the Mo atoms are in an octahedral environment in α-$CoMoO_4$ and MoO_3 oxides, they have similar electronic properties.[21] Due to the similarities in the electronic properties of MoO_3 and α-$CoMoO_4$, Ding et al. studied the cathodic performance of hydrothermally synthesized $CoMoO_4$ microcrystals in the voltage range 1.2−4.0 V and achieved reversible discharge capacity of 130 mAh g^{-1}.[19] Herein, we report the synthesis of α-$CoMoO_4$ submicrometer particles via polymer precursor

Received: November 5, 2012
Accepted: December 31, 2012
Published: December 31, 2012

method and its excellent Li-cycling behavior in the voltage range 0.005−3.0 V. Its electrochemical performance is compared with that of $CoMoO_4$ nanoplates prepared by citric acid assisted microwave synthesis.

EXPERIMENTAL SECTION

$CoMoO_4$ submicrometer particles were prepared by modifying the procedure reported by Pramanik et al.[23] Cobalt nitrate (2.9 g) and 2.4 g of sodium molybdate solution were separately dissolved in 100 mL of distilled water, and 5 mL of ammonia solution was added dropwise. The precipitate was filtered out, washed thoroughly, and dried. One g of the dried powder was dissolved in 100 mL of distilled water through complexation with ethylene diamine tetra-acetic acid (1.8 g), in the presence of diethanolamine (8 mL). A polymeric reagent, which is an aqueous solution mixture of polyvinyl alcohol (PVA) (1 g dissolved in 10 mL) and sucrose (10 g dissolved in 20 mL) were added to the above solution under hot conditions. The complete dehydration of the precursor solution generated a mesoporous carbon-rich mass. The precursor material was heat treated at 500 °C for 5 h in air to obtain the final product.

$CoMoO_4$ nanoplates were synthesized via citrate complex route assisted by microwave irradiation.[24] The citrate solution was prepared by dissolving appropriate molar ratios of citric acid in deionized water (30 g of citric acid in 100 mL of water). Stoichiometric amounts of cobalt nitrate and ammonium hepta molybdate were dissolved in citrate solution. The solution was made viscous by keeping it at a temperature of 100 °C for 1 h under constant stirring. The solution was placed in the microwave irradiation system and the reactions were performed under ambient air for 30 min (microwave irradiation (with 1200 W, 2.45 GHz) for 1 h with 1 min interval after every 1 min of operation). The obtained precursor was heated to 600 °C for 3 h to obtain the final product.

The compound was characterized by powder X-ray diffraction (XRD) (Philips X'PERT MPD, Cu Kα radiation). For morphology studies, scanning electron microscopy (SEM) (JEOL JSM-6700F, field emission electron microscope) and high-resolution transmission electron microscopy (TEM) (JEOL JEM 2100 operating at 200 kV) were employed. Raman spectra (Renishaw Raman system 2000) were recorded at room temperature.

The electrodes for Li-cycling were prepared by the doctor-blade technique using a mixture of the active material ($CoMoO_4$), Super P carbon (MMM Ensaco), and binder (Kynar 2801) in the mass ratio 70:15:15, using an etched Cu-foil (thickness 10 μm) as the current collector. The geometrical electrode area and mass of active material were 2 cm^2 and 2−3 mg, respectively. Coin-type test cells (size 2016) were assembled in an argon-filled glovebox (MBraun, Germany) and the cell components were Li metal (Kyokuto Metal Co., Japan) foil as counter electrode, glass microfiber filter (GF/F, Whatman Int.Ltd., Maidstone, England) as the separator, and 1 M $LiPF_6$ in ethylene carbonate (EC) and dimethyl carbonate (DMC) (1:1 by volume, Merck Selectipur LP40) as the electrolyte. The cyclic voltammetry and galvanostatic discharge−charge cycling of the cells were carried out at room temperature (25 °C) by computer-controlled MacPile II (Biologic, France) unit and Bitrode multiple battery tester (model SCN, Bitrode, USA), respectively. Details on electrode fabrication steps and sample handling for TEM are discussed in our previous study.[25]

RESULTS AND DISCUSSION

Structure and Morphology. The powder XRD pattern of the $CoMoO_4$ synthesized via polymer precursor method is shown in Figure 1 and it reveals the formation of compound in phase pure form with the monoclinic structure. The lattice parameter values a (Å) = 10.72, b (Å) = 8.95, c (Å) = 6.99, β = 115.63° are obtained by the Rietveld refinement and are in agreement with reported values of $CoMoO_4$ (JCPDS 21-0868).

Figure 2 displays the Raman spectra of the $CoMoO_4$ particles with peaks at 335, 364, 690, 817, 880, and 936 cm^{-1}. According

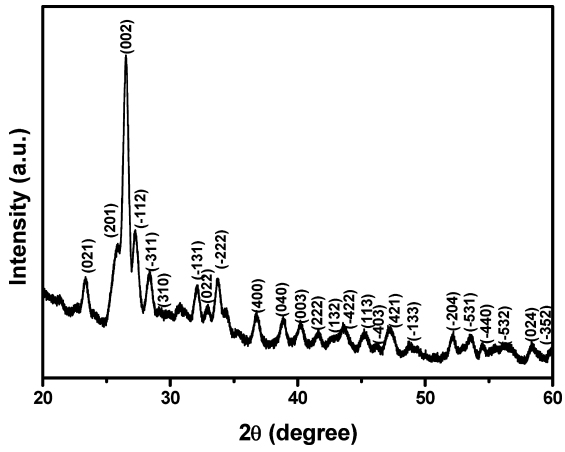

Figure 1. X-ray diffraction (XRD, Cu Kα radiation) pattern of α-$CoMoO_4$ submicrometer particles. Miller indices of α-$CoMoO_4$ are shown.

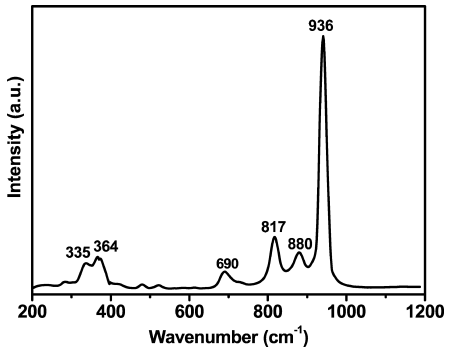

Figure 2. Raman spectra of α-$CoMoO_4$ submicrometer particles. Numbers refer to band positions in cm^{-1}.

to Pasquan et al.,[26] pure $CoMoO_4$ sample shows a strong band at 940 cm^{-1} and weaker bands at 700, 813, and 880 cm^{-1}. The Raman bands at 880 and 940 cm^{-1} and the broad band at 350 cm^{-1} can be assigned to Mo−O−Co stretching vibrations in cobalt molybdate.[27] The particle morphology was examined by SEM and TEM. Figure 3a, b, and c show that the $CoMoO_4$ powder consists of interconnected submicrometer size particles forming a porous network. The morphology is obtained from the simple polymer matrix based precursor solution. According to Pramanik et al.,[23] the polymer based synthesis approach helps to distribute the metal complexes throughout the viscous polymeric matrix, so that the complete evaporation of the precursor solution generates in situ a polar mesoporous carbonaceous material. In the presence of a small quantity (at 10%) of PVA, sucrose can gave rise to crushable, fluffy powder of the oxide system. The higher the fluffiness of the powders, the lower was the particle size. The fluffy mass obtained by the complete evaporation of precursor solution was thermolyzed at 500 °C for 5 h to get interconnected submicrometer size particles. Thus PVA provides a polymeric matrix structure for the cations and also provides heat through combustion of the carbonaceous material remaining of oxidized PVA.[23] Figure 3d shows the SAED (selected area electron diffraction) pattern consisting of bright spots with (201), (002), (−131), (040), (−532) planes. The inset in Figure 3d shows the HRTEM lattice image of $CoMoO_4$. The measured interplanar spacing matches well with the d-value corresponding to the (201) plane shown in the XRD pattern of the compound. Energy dispersive

dx.doi.org/10.1021/am302583c | ACS Appl. Mater. Interfaces 2013, 5, 918−923

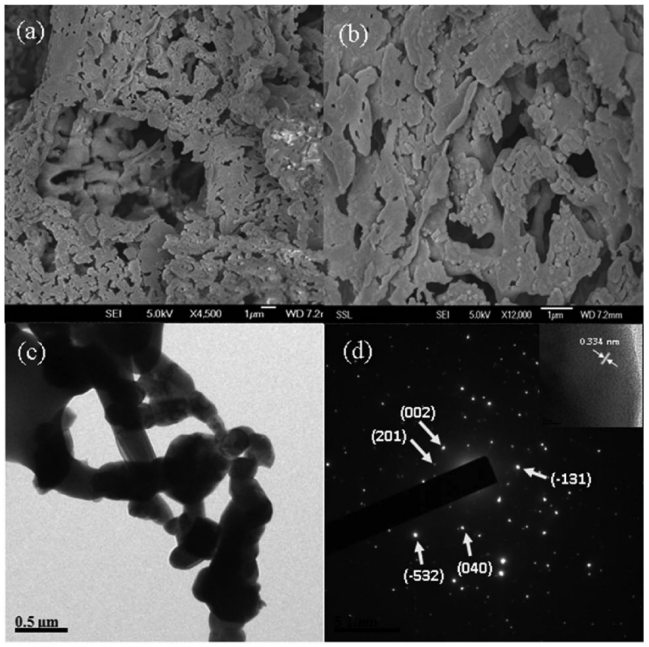

Figure 3. (a) SEM image of α-$CoMoO_4$ submicrometer particles. Scale bar is 1 μm. (b) SEM image of α-$CoMoO_4$ submicrometer particles. Scale bar is 1 μm. (c) TEM image of α-$CoMoO_4$ submicrometer particles. Scale bar is 200 nm. (d) SAED pattern of α-$CoMoO_4$ submicrometer particles. Miller indices are shown. Inset shows the HRTEM lattice image.

X-ray (EDX) elemental mapping has been used to evaluate the uniformity of distribution of cobalt, molybdenum, and oxygen elements. As shown in Figure 4, these three elements are distributed homogeneously in the selected portion of the sample at submicrometer scale.

$CoMoO_4$ prepared by citric acid assisted microwave synthesis shows nanoplate like morphology as shown in Figure 5a, and the corresponding SAED pattern is displayed in Figure 5b. The SAED patterns shows diffuse rings with many more diffraction spots than that of $CoMoO_4$ submicrometer particles (Figure 3d) which indicate better polycrystalline nanophase nature of $CoMoO_4$ nanoplates. Table 1 displays the BET surface area and average pore size obtained from N_2 absorption−desorption analysis. $CoMoO_4$ prepared by citric acid assisted microwave synthesis shows a specific surface area of 6.25 $m^2\ g^{-1}$ compared to 0.85 $m^2\ g^{-1}$ for $CoMoO_4$ via polymer matrix based precursor route. Average adsorption pore diameter ($4\ V/A$ where V is the pore volume and A is the surface area obtained from BET measurements) is calculated to be 15 and 160 nm for nano and micro-$CoMoO_4$, respectively.

Li-Cycling Studies. The Li-storage and cycling properties of $CoMoO_4$ were investigated by galvanostatic cycling in the voltage window 0.005−3.0 V vs Li at a current of 100 mA g^{-1}. Voltage vs capacity profiles of the selected cycles are shown in Figure 6. The first discharge curve starts from the open circuit voltage (OCV ≈ 2.5 V) and shows a sharp decrease to 1.3 V where a sloping voltage plateau sets in. This part comprises a capacity of 162 mAh g^{-1} which is equivalent to the uptake of 1.3 mols of Li (1 mol of Li corresponds to capacity of 122 mAh g^{-1}). The plateau is followed by a sloping region up to the 0.12 V yielding a capacity of 1184 mAh g^{-1}. A small voltage plateau can be seen at 0.12 V followed by continuous decrease in voltage up to the cut-off voltage, 0.005 V. Upon charging to 3 V, a smooth voltage profile is observed till 1.0 V which is followed by upward sloping voltage plateau up to ∼2.0 V and a gradual rise to 3.0 V. The initial discharge and charge capacities are 1355 and 1035 mAh g^{-1}, respectively. The irreversible capacity can be due to formation of solid electrolyte interphase (SEI) and an organic polymeric layer on the metal nanoparticles during first discharge.[28]

The theoretically expected capacity value for the first discharge reaction involving crystal structure destruction of α-$CoMoO_4$ and reduction of the Mo^{6+} to Mo^0 and Co^{2+} to Co is 980 mAh g^{-1}. An excess capacity of 55 mAh g^{-1} during first charge can be due to the extra Li-storage via an interfacial reaction due to the charge separation at the metal/Li_2O phase boundary.[29] First discharge to 0.005 V leads to crystal structure destruction followed by metal nanoparticles in an amorphous matrix of Li_2O as shown in eq 1. Equation 1 is not reversible

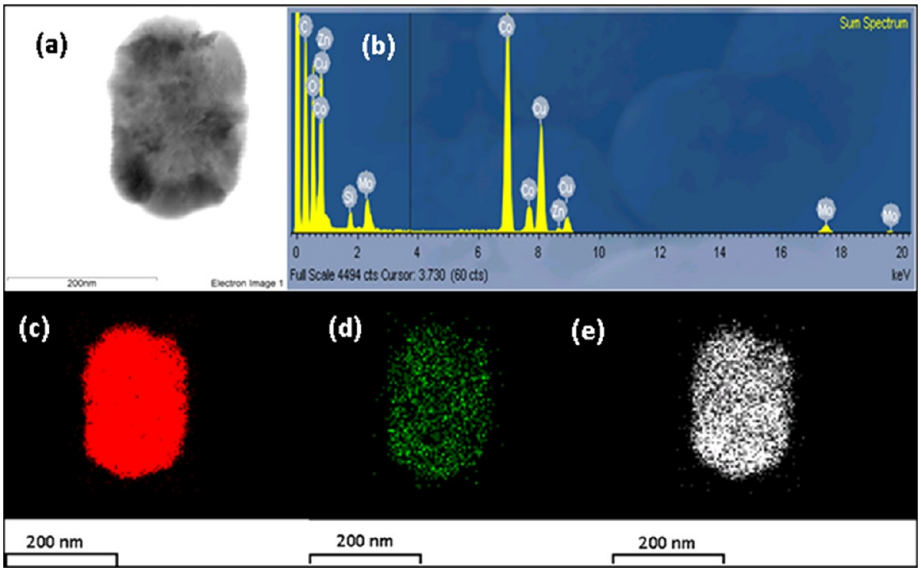

Figure 4. (a) SEM image of the portion selected for energy-dispersive X-ray (EDX) analysis. (b) EDX spectrum of the product. (c), (d), and (e) EDX maps of cobalt, molybdenum, and oxygen, respectively.

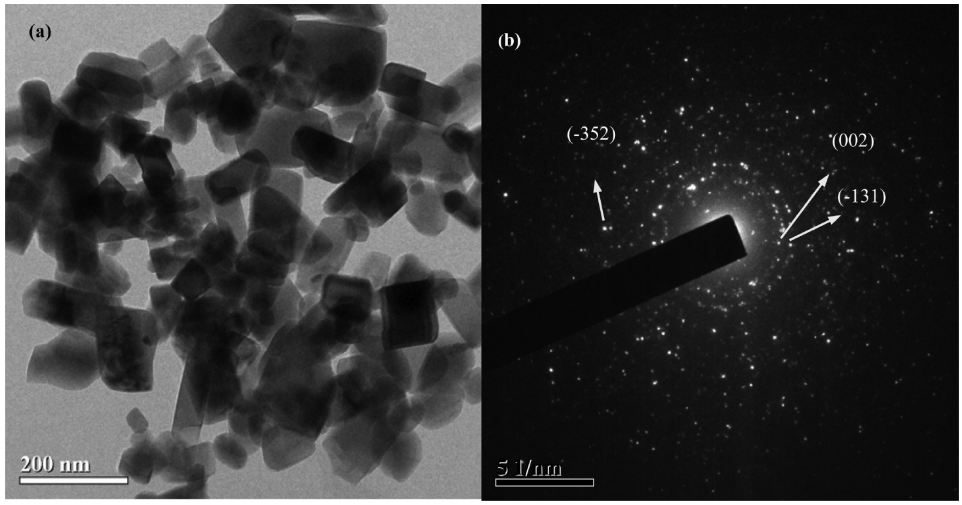

Figure 5. (a) TEM image of α-$CoMoO_4$ nanoplates. Scale bar is 200 nm. (b) SAED pattern of α-$CoMoO_4$ nanoplates. Miller indices are shown.

Table 1. BET Surface Area and Average Pore Size of $CoMoO_4$ Sample Prepared by Different Synthesis Routes

$CoMoO_4$ preparation method	BET surface area (m^2 g^{-1})	average pore size (nm)
polymer matrix precursor method	0.85 (±0.1)	160 (±2)
microwave synthesis	6.25 (±0.1)	15 (±2)

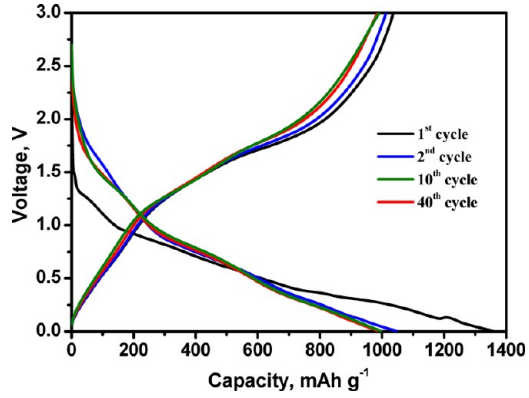

Figure 6. Galvanostatic charge–discharge profiles of α-$CoMoO_4$ submicrometer particles. Voltage range: 0.005–3 V vs Li; current: 100 mA g^{-1}.

due to the structure destruction and amorphization occurring during first discharge.

$$CoMoO_4 + 8Li \rightarrow Co + Mo + 4Li_2O \quad (8Li = 980\ mAh\ g^{-1}) \tag{1}$$

During subsequent charge–discharge cycles, the expected reversible capacity is 980 mAh g^{-1}, if the following reactions happen:

$$Co + Li_2O \leftrightarrow CoO + 2Li \quad (2Li = 245\ mAh\ g^{-1}) \tag{2}$$

$$Mo + 3Li_2O \leftrightarrow MoO_3 + 6Li \quad (6Li = 735\ mAh\ g^{-1}) \tag{3}$$

Figure 7 illustrates the capacity vs cycle number plots extracted from galvanostatic cycling data. Assuming 1 C = 980 mA g^{-1}, the applied current corresponds to a current rate

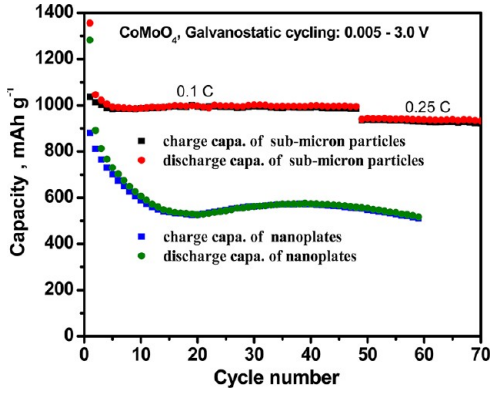

Figure 7. Capacity vs cycle number plot of α-$CoMoO_4$ at various C-rates. Voltage range: 0.005–3 V vs Li.

of 0.1 C. A high reversible capacity of 990 (±10) mAh g^{-1} is obtained with 100% capacity retention between 5 and 50 cycles. When the current is increased to 0.25 C, a stable capacity of 940 mAh g^{-1} is delivered. For comparison, nanoplates of $CoMoO_4$ are prepared by citric acid complex route assisted by microwave irradiation,[24] and their Li-cycling behavior has been investigated. As can be seen from Figure 7, nanoplates of $CoMoO_4$ show a drastic capacity fading for the first 15 cycles, and a reversible capacity of 560 mAh g^{-1} is obtained after 50 cycles. The observed decrease in reversible capacity during initial 15 cycles (and subsequent increase and stabilization) can be attributed to the "formation" or "conditioning" of the electrode during which the formation of stable solid electrolyte interphase (SEI) on the metal nanoparticles, the percolation of the electrolyte through the active material, i.e. Co, Mo/Li_2O amorphous composite, and the establishment of an intimate electronic contact of the composite with the current collector occur.[25] $CoMoO_4$ nanoplate composite electrodes need several cycles to complete the "conditioning" phase whereas interconnected $CoMoO_4$ submicrometer particles efficiently overcome this phase without any capacity loss. This superior electrochemical performance can be attributed to the unique morphology obtained by the "polymer matrix based metal precursor" synthetic method set forth by Pramanik et al.[23] The stable electrochemical performance of the interconnected submicrometer particles can also be due to the synergistic

dx.doi.org/10.1021/am302583c | ACS Appl. Mater. Interfaces 2013, 5, 918–923

effect between CoO and MoO_3 during cycling. The unique morphology of $CoMoO_4$, in which primary particles are mutually interconnected, has been considered beneficial for the electrochemical performance. It assures a suitable electrical conductivity and mechanical strength on a long extended electrode cycling.[30]

Cyclic voltammetry is a complementary technique to galvanostatic cycling and helps in understanding the redox potentials at which the discharge−charge reactions occur. Figure 8 shows the CV curves of $CoMoO_4$ submicrometer

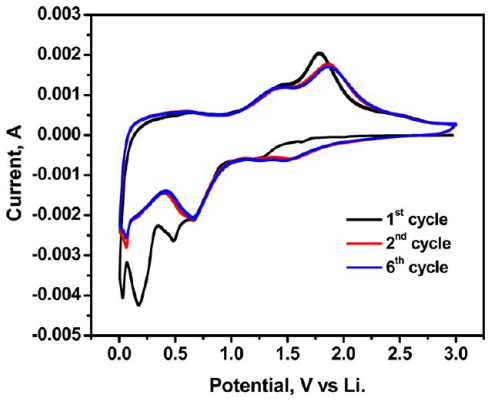

Figure 8. Cyclic voltammogram of α-$CoMoO_4$ submicrometer particles. Potential window, 0.005−3 V; scan rate 58 μV s^{-1}. Li metal was the counter and reference electrode.

particles in the potential window 0.005−3 V at the scan rate 58 μV sec^{-1}. It is clear from the CV curves that there is substantial difference between the first and subsequent cycles. The first cathodic scan results in a shoulder peak at 0.67 V, broad peaks at ∼0.5 and 0.18 V, and a sharp peak at a potential close to 0.005 V. The peaks at 0.5 and 0.18 V are not seen in subsequent cycles. This can be due to the unique reactions happening during first discharge as shown in eq 1. These two irreversible peaks during first cathodic scan are due to the crystal structure destruction accompanied by the complete reduction to Co^0 and Mo^0 metal nanoparticles and the formation of solid electrolyte interface (SEI) due to the reduction of solvents in the electrolyte. The first anodic scan shows two peaks at 1.4 and 1.8 V which correspond to oxidation of Co and Mo to form CoO and MoO_3. The peak at 1.4 V can be attributed to the oxidation of Mo^0 to Mo^{4+}, whereas the peak at 1.8 V can be due to the oxidation of Co to Co^{2+} and Mo^{4+} to Mo^{6+}.[16,31,32] They became broadened during further cycles. Second and further cathodic scans show peaks at 0.05, 1.56, and 0.66 V, while the anodic scans show peaks at 1.4 and 1.85 V. The curves corresponding to the second and sixth scans overlap, indicating the reversibility of the eqs 2 and 3 and hence the capacity stability.

To investigate the nature of the products formed upon cycling, ex situ XRD and TEM studies were carried out on several duplicate cells. Ex-situ TEM image (Figure 9a) indicates that after two discharge−charge cycles, the micrometer-sized particles are broken down into particles of size 40 nm. The SAED patterns of the different portions of the sample collected from the electrode charged to 3 V after two galvanostatic charge−discharge cycles are shown in Figure 9b and c. The SAED pattern in Figure 9b shows sharp distinct spots, whereas that in Figure 9c shows diffuse spots/rings. It can be confirmed that there exists both crystalline and nanoamorphous phases

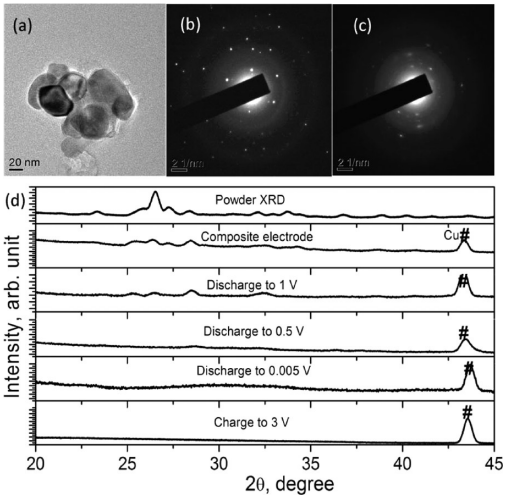

Figure 9. (a) TEM image of particles of cycled electrodes of α-$CoMoO_4$ submicrometer particles (2nd cycle; charged to 3 V). (b) and (c) SAED pattern of different regions. (d) XRD spectra of cycled α-CoMoO4 electrode.

after first 2 discharge−charge cycles. The *d*-values, 2.50 (±0.05), 2.62 (±0.05), and 1.65 (±0.05) Å, derived by measuring the diameter of rings/spots about the center, can be assigned to the (101), (002), and (110) planes of hexagonal CoO (JCPDS 89-2803). The calculated *d*-values, 3.84 (±0.05), 3.29 (±0.05), and 2.95 (±0.05) Å can be assigned to the (100), (011), and (101) planes of monoclinic MoO_3 (JCPDS 85-2405). Figure 9d shows the XRD patterns of $CoMoO_4$ powder, bare $CoMoO_4$ composite electrode, electrode after discharging to 1, 0.5, and 0.005 V, and in the charged state (3 V). The diffraction line due to compound completely disappears in the XRD patterns of the electrodes discharged to 0.5 and 0.005 V, indicating initial crystal structure destruction and amorphization. The XRD pattern of the electrode charged to 3 V does not show any peak which indicates that the initial crystalline compound is not reformed during charging, and the reversible reactions (eqs 2 and 3) involve amorphous nanophase materials. So it can be deduced that nanophase, amorphous CoO and MoO_3 are undergoing conversion reaction/displacement redox reaction as shown in eqs 2 and 3. It should be kept in mind that there is no experimental proof for the "conversion" reaction of MoO_3 (eq 3) where Mo^{6+} will be converted to Mo metal nanoparticles during deep discharge and MoO_3 will be reformed upon charging to 3 V. In the literature, it is assumed that high reversible capacity value delivered by MoO_3 during cycling in voltage range 0−3 V can be due to the reformation of MoO_3 by the uptake of 6 mols of Li per formula unit.[16,33] More sophisticated techniques are needed to prove the formation of Mo^{6+} from Mo metal nanoparticles.

In summary, $CoMoO_4$ particles have been prepared from the complete evaporation of a polymer matrix based metal−complex precursor solution and subsequent heat treatment. The product has been characterized by X-ray diffraction, scanning electron microscopy, high-resolution transmission electron microscopy, and Raman spectroscopy. Interconnected networks of submicrometer size α-$CoMoO_4$ particles were obtained. The Li storage and cycling properties were examined in the voltage range 0.005−3.0 V vs Li at 100 mA g^{-1}, and compared to α-$CoMoO_4$ nanoplates synthesized by citrate complex route assisted by microwave irradiation. Li-reaction

dx.doi.org/10.1021/am302583c | ACS Appl. Mater. Interfaces 2013, 5, 918−923

mechanism of α-$CoMoO_4$ submicrometer particles has been investigated by ex-situ XRD and HR-TEM. The material exhibits a high reversible capacity of 990 mAh g^{-1}, at 0.1 C, which is stable up to 50 cycles. The excellent cycling stability can be attributed to the unique morphology of interconnected micrometer size particles, thus making α-$CoMoO_4$ a promising anode material for Li-ion batteries.

AUTHOR INFORMATION

Corresponding Author

*E-mail: phychowd@nus.edu.sg.

Notes

The authors declare no competing financial interest.

REFERENCES

(1) Yoshio, M.; Brodd, R. J.; Kozawa, A. *Lithium-Ion Batteries: Science and Technologies*; Springer: New York, 2009.

(2) Aifantis, K. E.; Hackney, S. A.; Kumar, R. V. *High Energy Density Lithium Batteries: Materials, Engineering, Applications*; Wiley-VCH, 2010.

(3) Wang, F.; Robert, R.; Chernova, N. A.; Pereira, N.; Omenya, F.; Badway, F.; Hua, X.; Ruotolo, M.; Zhang, R.; Wu, L.; Volkov, V.; Su, D.; Key, B.; Whittingham, M. S.; Grey, C. P.; Amatucci, G. G.; Zhu, Y.; Graetz, J. *J. Am. Chem. Soc.* **2011**, *133*, 18828−18836.

(4) Poizot, P.; Laruelle, S.; Grugeon, S.; Dupont, L.; Tarascon, J. M. *Nature* **2000**, *407*, 496−499.

(5) Sharma, N.; Shaju, K. M.; Subba Rao, G. V.; Chowdari, B. V. R.; Dong, Z. L.; White, T. J. *Chem. Mater.* **2003**, *16*, 504−512.

(6) Tao, T.; Glushenkov, A. M.; Zhang, C.; Zhang, H.; Zhou, D.; Guo, Z.; Liu, H. K.; Chen, Q.; Hu, H.; Chen, Y. *J. Mater. Chem.* **2011**, *21*, 9350−9355.

(7) Fang, X.; Guo, B.; Shi, Y.; Li, B.; Hua, C.; Yao, C.; Zhang, Y.; Hu, Y.-S.; Wang, Z.; Stucky, G. D.; Chen, L. *Nanoscale* **2012**, *4*, 1541−1544.

(8) Xia, F.; Hu, X.; Sun, Y.; Luo, W.; Huang, Y. *Nanoscale* **2012**, *4*, 4707−4711.

(9) Young, A. P.; Schwartz, C. M. *Science* **1963**, *141*, 348−349.

(10) Li, Y.; Tan, S.; Jiang, J.; Huang, Z.; Tan, X. *CrystEngComm* **2011**, *13*, 2649−2655.

(11) Cui, J.-X.; Wang, W.-S.; Zhen, L.; Shao, W.-Z.; Chen, Z.-L. *CrystEngComm* **2012**, *14*, 7025−7030.

(12) Raju, G. S. R.; Pavitra, E.; Ko, Y. H.; Yu, J. S. *J. Mater. Chem.* **2012**, *22*, 15562−15569.

(13) Peng, C.; Gao, L.; Yang, S.; Sun, J. *Chem. Commun.* **2008**, 5601−5603.

(14) Zhou, L.; Yang, L.; Yuan, P.; Zou, J.; Wu, Y.; Yu, C. *J. Phys. Chem. C* **2010**, *114*, 21868−21872.

(15) Sen, U. K.; Mitra, S. *RSC Adv.* **2012**, *2*, 11123−11131.

(16) Meduri, P.; Clark, E.; Kim, J. H.; Dayalan, E.; Sumanasekera, G. U.; Sunkara, M. K. *Nano Lett* **2012**, *12*, 1784−8.

(17) Leyzerovich, N. N.; Bramnik, K. G.; Buhrmester, T.; Ehrenberg, H.; Fuess, H. *J. Power Sources* **2004**, *127*, 76−84.

(18) Kim, S.-S.; Ogura, S.; Ikuta, H.; Uchimoto, Y.; Wakihara, M. *Solid State Ionics* **2002**, *146*, 249−256.

(19) Ding, Y.; Wan, Y.; Min, Y.-L.; Zhang, W.; Yu, S.-H. *Inorg. Chem.* **2008**, *47*, 7813−7823.

(20) Xu, Z.; Li, Z.; Tan, X.; Holt, C. M. B.; Zhang, L.; Amirkhiz, B. S.; Mitlin, D. *RSC Adv.* **2012**, *2*, 2753−2755.

(21) Robertson, L.; Duttine, M.; Gaudon, M.; Demourgues, A. *Chem. Mater.* **2011**, *23*, 2419−2427.

(22) Livage, C.; Hynaux, A.; Marrot, J.; Nogues, M.; Ferey, G. *J. Mater. Chem.* **2002**, *12*, 1423−1425.

(23) Pramanik, P. *Bull. Mater. Sci.* **1999**, *22*, 335−339.

(24) Ryu, J. H.; Koo, S.-M.; Yoon, J.-W.; Lim, C. S.; Shim, K. B. *Mater. Lett.* **2006**, *60*, 1702−1705.

(25) Cherian, C. T.; Reddy, M.; Subba Rao, G. V.; Sow, C. H.; Chowdari, B. V. R. *J. Solid State Electrochem.* **2012**, *16*, 1823−1832.

(26) Villa, P. L.; Trifirò, F.; Pasquon, I. *React. Kinet. Catal. Lett.* **1974**, *1*, 341−344.

(27) Herrera, J. E.; Resasco, D. E. *J. Phys. Chem. B* **2003**, *107*, 3738−3746.

(28) Cherian, C. T.; Sundaramurthy, J.; Kalaivani, M.; Ragupathy, P.; Kumar, P. S.; Thavasi, V.; Reddy, M. V.; Sow, C. H.; Mhaisalkar, S. G.; Ramakrishna, S.; Chowdari, B. V. R. *J. Mater. Chem.* **2012**, *22*, 12198−12204.

(29) Zhukovskii, Y. F.; Balaya, P.; Kotomin, E. A.; Maier, J. *Phys. Rev. Lett.* **2006**, *96*, 058302.

(30) Vidal-Abarca, C.; Lavela, P.; Tirado, J. L. *J. Phys. Chem. C* **2010**, *114*, 12828−12832.

(31) Zhou, L.; Zhao, D.; Lou, X. W. *Adv. Mater.* **2012**, *24*, 745−8.

(32) Wang, Y.; Park, J.; Sun, B.; Ahn, H.; Wang, G. *Chem.– Asian J.* **2012**, *7*, 1940−1946.

(33) Tao, T.; Glushenkov, A. M.; Zhang, C.; Zhang, H.; Zhou, D.; Guo, Z.; Liu, H. K.; Chen, Q.; Hu, H.; Chen, Y. *J. Mater. Chem.* **2011**, *21*, 9350.